Journal of Hydrology 575 (2019) 755–766

Contents lists available at ScienceDirect

Journal of Hydrology

journal homepage: www.elsevier.com/locate/jhydrol

Research papers

Remote impacts of typhoons on the hydrodynamics, sediment transport and bed stability of an intertidal wetland in the Yangtze Delta

S.L. Yang[a,1,*], J.Q. Fan[a,1], B.W. Shi[a,*], T.J. Bouma[b], K.H. Xu[c,d], H.F. Yang[e], S.S. Zhang[a], Q. Zhu[f], X.F. Shi[g]

[a] State Key Laboratory of Estuarine and Coastal Research, East China Normal University, Shanghai 200241, China
[b] Royal Netherlands Institute for Sea Research (NIOZ), Department of Estuarine and Delta Systems, and Utrecht University, P.O. Box 140, 4400 AC Yerseke, the Netherlands
[c] Department of Oceanography and Coastal Sciences, Louisiana State University, Baton Rouge, LA 70803, USA
[d] Coastal Studies Institute, Louisiana State University, Baton Rouge, LA 70803, USA
[e] Survey Bureau of Hydrology and Water Resources of the Changjiang Estuary, Bureau of Hydrology, Changjiang Water Resources Commission, Shanghai 200136, China
[f] Institute of Environmental and Ecological Engineering, Guangdong University of Technology, Guangzhou 510006, China
[g] Key Laboratory of Marine Sedimentology and Environmental Geology, First Institute of Oceanography, State Oceanic Administration, Qingdao 266061, China

ARTICLE INFO

This manuscript was handled by Marco Borga, Editor-in-Chief, with the assistance of George Constantinescu, Associate Editor

Keywords:
Typhoon
Mudflat
Saltmarsh
Intertidal wetland
Storm impact
Yangtze Delta

ABSTRACT

Intertidal wetlands are widely considered to be vulnerable to storm impacts. While much attention has been given to the effect of hurricane/typhoon landfall on local erosion/deposition in intertidal wetlands, less is known about how distant hurricanes/typhoons can affect an intertidal wetland or about the comprehensive effects of hurricanes/typhoons on hydrodynamics, sediment transport and seabed stability. Here, we investigate the possible impacts of thirteen typhoons that occurred in the western Pacific during summer–autumn 2016 on an intertidal wetland in the Yangtze Delta. We detected the impacts from eight of the typhoons during half of their duration when these typhoons were 450–2000 km away (nearest distance ever for each typhoon) from the delta. These remote typhoons caused 2–5 times maximum increases in hydrodynamics and suspended sediment concentration. Correspondingly, considerable net mudflat erosion and marsh deposition were observed. We therefore conclude that intertidal wetlands can be strongly affected by typhoons, even those passing by hundreds of kilometres away. These findings contribute to understand how far and in what extent hurricanes/typhoons can affect intertidal wetlands and to increase knowledge needed for coastal management.

1. Introduction

Intertidal wetlands are among the world's most valuable ecosystems (Costanza et al., 1997), because they provide important ecosystem functions and services (Barbier et al., 2011; Kirwan and Megonigal, 2013; Temmerman et al., 2013). The environmental stability of intertidal wetlands is presumably a key factor for the health of this ecosystem. The long-term stability of intertidal wetlands is influenced by sediment supply and relative sea-level changes (Blankespoor et al., 2014; Yang et al., 2018). Its responses to fluvial sediment decline, land subsidence and global sea-level rise has been widely addressed (Yang et al., 2005; Blum and Roberts, 2009; Kirwan, and Megonigal; Schuerch et al., 2018). The short-term stability of intertidal wetlands is strongly disturbed by storms. Tropical cyclones (hurricanes/typhoons) are extreme storms that frequently impact the coasts of the Pacific, Atlantic and India Oceans (Emanuel, 2005; Knutson et al., 2010). Although there is great uncertainty about whether or not the frequency of tropical cyclones will increase, most studies show that the tropical cyclone intensity should increase as the climate warms (Webster et al., 2005; Sobel et al, 2016). Intertidal wetlands are widely considered to be vulnerable to storm attack (Leonardi et al., 2016). However, most previous studies have focused on the strong erosion/accretion caused by hurricanes/typhoons when they landed at the intertidal wetlands (Yang et al., 2003; Turner et al., 2006; Williams and Flanagan, 2009; Van Ormondt et al., 2015; Liu et al., 2017). In contrast, less is known about the remote effect of hurricanes/typhoons or about their comprehensive effects on hydrodynamics, sediment transport and erosion/accretion. There is a great need to strengthen research in these fields because the sphere of influence of hurricanes/typhoons may be much greater than their landing area and because the aspects of storm impact

* Corresponding authors.
E-mail addresses: slyang@sklec.ecnu.edu.cn (S.L. Yang), bwshi@sklec.ecnu.edu.cn (B.W. Shi).
[1] These authors contributed equally to this work.

https://doi.org/10.1016/j.jhydrol.2019.05.077
Received 2 December 2018; Received in revised form 16 March 2019; Accepted 25 May 2019
Available online 25 May 2019
0022-1694/

may be much more than the bed-level change.

Here, we bridge the above knowledge gap by studying the Yangtze Delta as a model system because it is one of the world's largest deltas in terms of size, and its intertidal wetland areas are known to be typically affected each summer by typhoons (Wang et al., 2016, 2018; Zhu et al., 2017). Through combination of qualitative description and quantitative analysis, we attempt to: (1) Divide the remote typhoons or typhoon durations into two parts, i.e., the impacting and non-impacting ones; (2) Address the quantitative characteristics of the impacting typhoons; (3) Quantify the magnitudes of the average and maximum typhoon impacts; and (4) Develop an impact factor for quantitative relationship between a remote typhoon and its impact. This study is unique in that it focuses on how many typhoons that form in the Pacific Ocean and during how long duration they affect the wetlands in this delta, the quantitative characteristics of the impacting typhoons (i.e., their strength and distance from the delta), and the comprehensive effects of typhoons, including the hydrodynamic mechanism, sediment transport and bed-level and marsh changes, based on high temporal-resolution field measurements.

2. Materials and methods

2.1. Data mining

Data of typhoon tracks and maximum wind speeds near the typhoon centers during the typhoon season (July through September) in 2016 were obtained from the National Meteorological of China (http://www.nmc.cn/). The 3-hourly wind speed and 6-hourly wave height data at the nearshore station in the Yangtze Delta during the same period were obtained from the European Centre for Medium-Range Weather Forecasts (https://www.ecmwf.int/). The astronomical tide data were provided by the East China Sea Branch of State Oceanic Administration.

2.2. Field observations

Field observations were carried out using a tripod system from August 29 to September 28, 2016, on a tidal wetland in the Yangtze Delta front (Fig. 1). The winds in the Yangtze Delta are influenced by monsoons and typhoons, and the multi-year average of wind speed is ca. 4 m/s (Yang et al., 2008). The tides in this area are mixed semi-diurnal, with a mean tidal range of 3.2 m in our study site (Gao et al., 2008). The intertidal area is approximately 900 m in width, which consists of a salt marsh (upper 150 m) and a mudflat (lower 750 m) (Fig. 1c). The observation site is below the mean sea level (MSL) and 650 m seaward from the seawall.

An SBE 26plus Seagauge Wave and Tide Recorder (4 Hz) (Sea–Bird Electronics Inc., USA) was mounted horizontally on the bed surface to measure the wave parameters and water depth at an interval of 10 min (the burst lasted for 256 s and conducted 1024 measurements). An Aquadopp HR–Profiler (1 Hz) (Nortek, Norway) was deployed on a tripod, and its downward-facing probe was at a height of 0.7 m above the seabed to measure the current profile. An Alec Current Meter (1 Hz) (Alec Electronics, Japan) was attached to the tripod to measure the point currents at a height of 0.5 m. The currents were measured at an interval of 5 min. An Argus Surface Meter IV (ASM) (5 Hz) (Argus, Germany), which has an array of sensors with a measuring profile of approximately 1 m, was mounted to obtain the turbidity profile at an interval of 2.5 min (Fig. 2).

The elevations along the cross-shore intertidal wetland profile were surveyed before and after typhoons, using a high-resolution, high-accuracy, real-time kinematic global-positioning-system unit (Trimble Company, USA) with horizontal and vertical errors of ± 2 mm. All surveys were based on the same reference benchmark that was built into a concrete seawall at the starting point of the central cross-shore profile, and all repeated surveys of elevation were conducted at fixed sites on the wetlands. To avoid the influence of the footprints on the results of surveys, we were careful not to trample on the soft soils at the survey points. While reading the elevation, we held the RTK-GPS and placed it just onto the sediment surface, preventing it from sinking into the soils. Water samples were acquired at the observation site for suspended sediment concentration (SSC) calibration. Surficial bed sediments were collected each day during the ebb period to measure the water content and the grain size. We used a buried-plate method to measure relative bed-level changes between tidal cycles (Zhu et al., 2017). To avoid the disturbance of the tripod, the buried-plate site was 5 m away from the tripod in the longshore direction. Specifically, we buried a square ceramic tile 0.3 m beneath the sediment surface. Then, we smoothed the sediment surface to be consistent with the surrounding areas. The first measurement was performed two tidal cycles after burial of the tile, by which time the mudflat had been restored to its undisturbed state. We measured the distance between the sediment surface and the plate using 16 thin sticks inserted vertically into the sediment. To minimize the impact from the ripples, we positioned eight sticks on ripple crests and a further eight within ripple troughs. Relative bed-level changes were calculated from the difference between the two measurements.

2.3. Data processing

In situ turbidity data obtained from the ASM were converted to suspended sediment concentration data via a calibration equation in the laboratory using water samples collected in situ (Fig. 3). Grain size analyses were measured in laboratory for the surficial sediment samples using a Laser Diffraction Particle Size Analyzer, Coulter LS100Q (Coulter Inc., USA), after removal of organic matter to obtain the grain size distribution curves of the sediment. Mean bed shear stress caused by combined wave-current action (τ_{cw}) during 10-min periods and critical shear stress for the erosion of bottom sediment (τ_e) were computed (see details in Appendix A) to study sediment transport and bed-level changes.

To quantifiably describe the potential impacts of a remote typhoon on coastal meteorological hydrodynamics, we developed a dimensionless impact factor of a typhoon (IF_T), which was defined as

$$IF_T = \frac{100 S_T}{D_{T\hat{A}\text{-}C}} \quad (1)$$

where S_T is the maximum wind speed near the typhoon center (m/s), $D_{T\text{-}C}$ is the distance between the typhoon center and the coast (km), the number 100 is used to ensure that the IF_T values range from 1 to 10. This factor is based on the assumption that a typhoon impact is mainly determined by the wind speed of the typhoon center and the distance between the typhoon and the coast, and that IF_T is proportional to S_T but inversely proportional to $D_{T\text{-}C}$. Correlations between IF_T and wind speed (WS_Y) and wave height (H_N) in the Yangtze Delta were established, and the significance levels of the correlations were tested, using regression approaches.

To investigate the time lag in WS_Y and H_N after IF_T, we established correlations with time lags of 1–5 tides, and compared their correlation coefficients with the correlation coefficient of the in-phase correlation. We selected the correlation with the highest correlation coefficient. We defined the time lag as that has the highest correlation coefficient.

The rate at which the wave group as a whole travels across the open ocean between the typhoon and the coast was calculated using the following equation:

$$C_g = gT/(4\pi) \quad (2)$$

where g is the acceleration of gravity, T is the wave period, and π is the circumference ratio (Komar, 1976).

3. Results and discussion

During July through September 2016, thirteen typhoons were

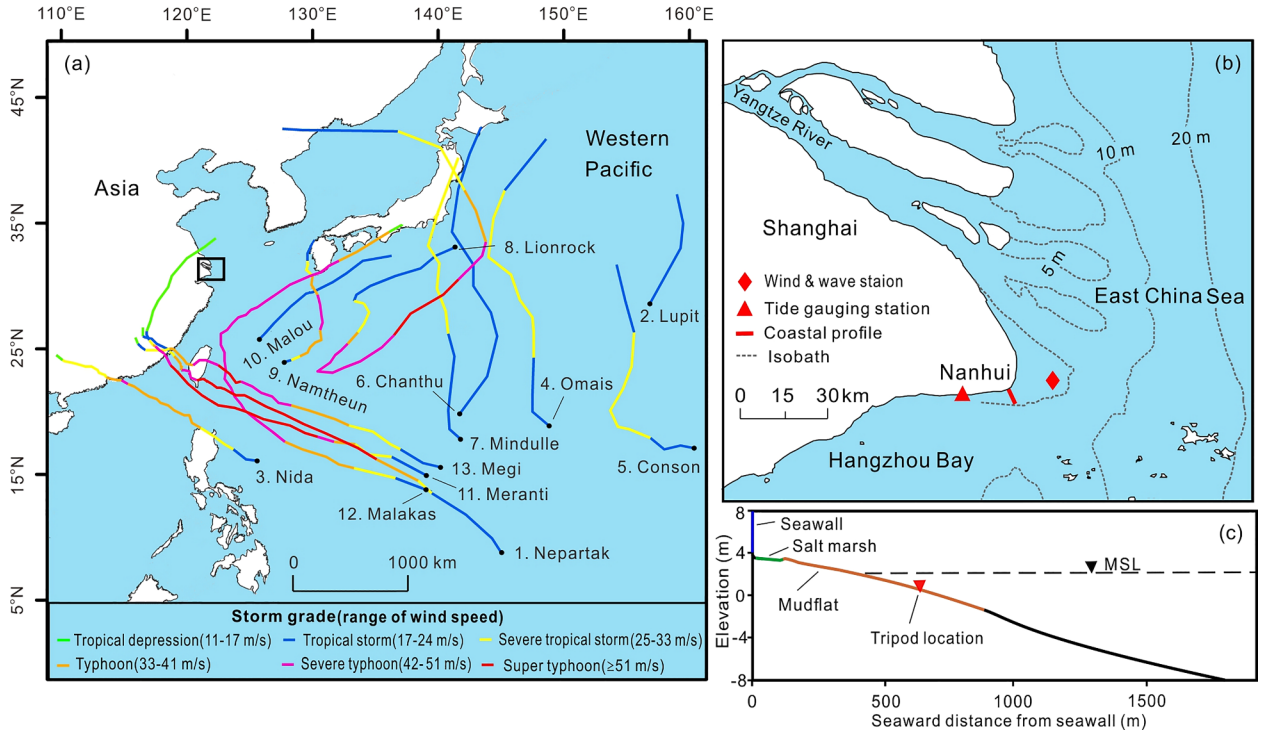

Fig. 1. Study area. (a) The northwestern Pacific showing the tracks of typhoons, each begun at the black point. (b) The Yangtze Delta showing the locations of wind, wave and tide gauging stations and studied intertidal wetland. Dashed lines are isobaths in meters. (c) Cross-shore wetland profile showing the site of tripod measurements. Elevation is based on the lowest astronomical tide. MSL: Mean sea level.

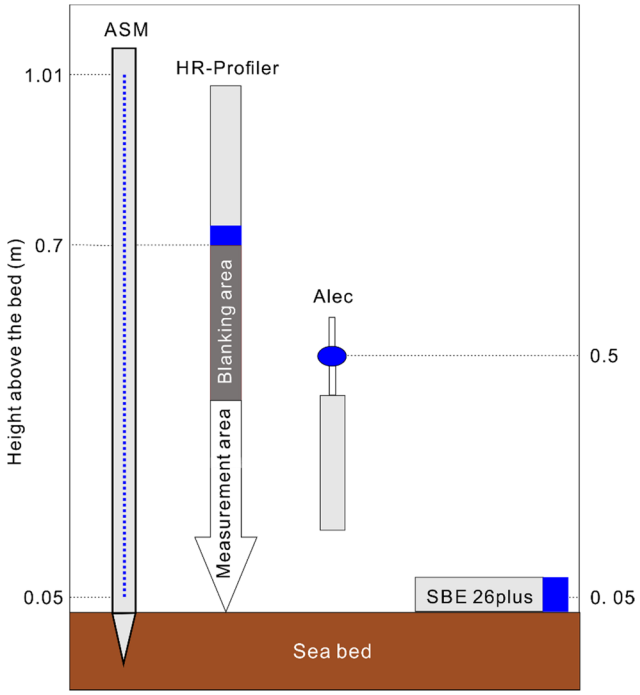

Fig. 2. Schematic figure of instrument deployment on a tripod. Blue parts indicate the locations of instruments' sensors. See tripod location in Fig. 1c.

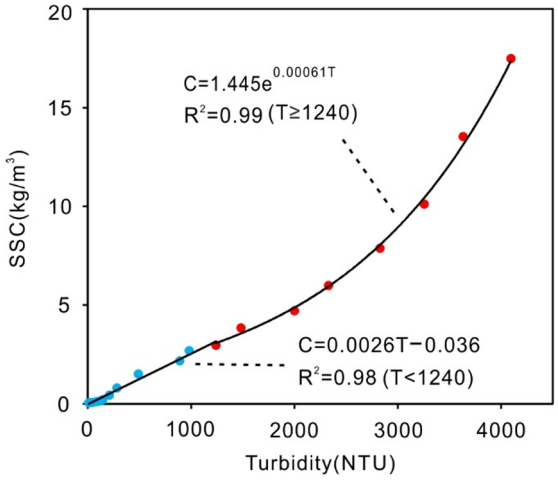

Fig. 3. Calibrated regression relationship between turbidity (T) measured by ASM and SSC (C) in the laboratory. R^2 is correlation coefficient. NTU is Nephelometric Turbidity Unit. Blue and red dots represent low and high turbidities, respectively.

formed and moved northwestward through the western Pacific (Fig. 1). The maximum sustained wind speed near the typhoon center ranged from 17 to 70 m/s, the typhoon circle radius of 17 m/s wind speed was between 100 and 600 km, and the distance between the typhoon center and the Yangtze Delta varied from 200 to 4000 km (Fig. 4a). The duration of these typhoons together amounted to 65% of time of the three months.

3.1. Remote impacts of typhoons on coastal winds

At the Yangtze Delta, the tide-averaged wind speed ranged from 1.5 to 8.4 m/s (4.8 m/s on average) during the non-typhoon periods. Among the 115 tides when one or two typhoons were moving across the Pacific Ocean, 10 tides were accompanied by wind speeds higher than the maximum wind speed during non-typhoon periods. The wind speeds during these 10 tides were 10 m/s on average (Fig. 4b, Table S1). During these 10 tides, the wind speed at the Yangtze Delta were most likely influenced by typhoons. On average, the < 6.5 m/s wind speeds at the Yangtze Delta in the typhoon periods were equal to the wind speeds in the non-typhoon periods. Thus, the 6.5–8.4 m/s wind speeds at the Yangtze Delta in the typhoon periods may also have been

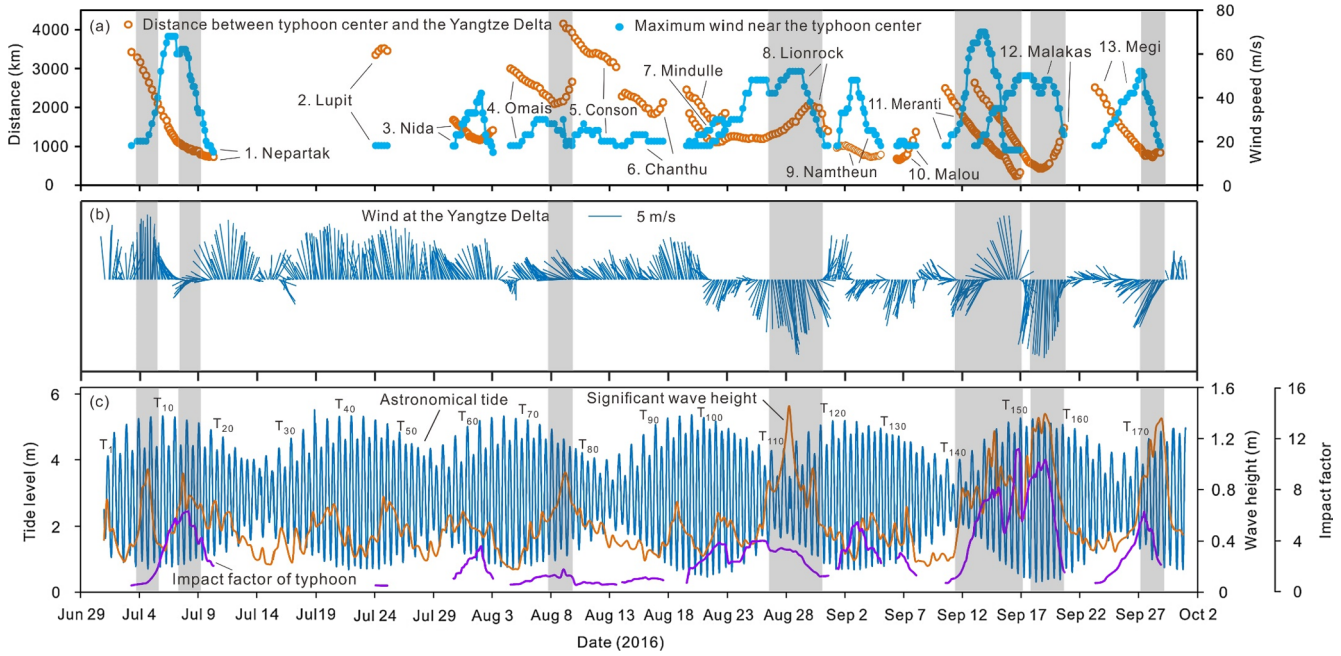

Fig. 4. Time series of remote typhoon information, and wind, tide and wave at the nearshore station in the Yangtze Delta front. (a) distance between typhoon center and Yangtze Delta, and maximum wind speed near typhoon center, (b) wind vector at the Yangtze Delta and (c) astronomical tidal level, nearshore significant wave height and impact factor of typhoon. Gray background bars indicate the periods when the impacts of the typhoons on the Yangtze Delta were significant. See Appendix B (Table S1) for more details.

influenced by typhoons. These wind speeds were observed during 22 tides (Table S1). Therefore, we conclude that the wind speeds at the Yangtze Delta were more or less influenced by typhoons during 32 tides, or 28% of the duration of the typhoon periods.

During the impacting typhoons, defined as the periods when a typhoon impact on wind speed in the Yangtze Delta was detected, the distance between the typhoon center and the Yangtze Delta ($D_{T\text{-}Y}$), the maximum wind speed near typhoon center (WS_T), the impact factor of typhoon (IF_T) and the wind speed in the Yangtze Delta (WS_Y) were on average 1650 km, 38 m/s, 4.4 and 8.4 m/s, respectively. During the non-impacting typhoons, defined as the periods when a typhoon impact on the Yangtze Delta was undetected, the values of $D_{T\text{-}Y}$, WS_T, IF_T and WS_Y were on average 1800 km, 29 m/s, 2.2 and 4.8 m/s (equal to the mean wind speed under no typhoon conditions), respectively. During the impacting typhoons, the correlation between WS_Y and IF_T was statistically significant ($R^2 = 0.35$ and $p < 0.001$ for all the impacting periods, and R^2 ranging from 0.70 to 0.99 and $p < 0.001$, for the three individual typhoon events) (Fig. S1). However, there was no significant correlation between WS_Y and IF_T ($R^2 = 0.009$, $p = 0.4$) during the non-impacting typhoons (data shown in Table S1).

In addition to increasing wind speed, typhoons often changed wind direction and sometimes reduced wind speed at the Yangtze Delta. This is because in summer, the monsoon-induced winds in the East China Sea are typically northward or northwestward (Fig. 4b; Sun et al., 2016). On the other hand, the typhoon-generated winds at the Yangtze Delta tended to be southwestward or southward (Fig. 4b) because the typhoons were often to the southeast or east of the Yangtze Delta (Fig. 1) and because typhoon systems rotate counter-clockwise in the Northern Hemisphere (Bridges, 1987). Thus, at the beginning and end of the typhoon impact, the winds at the Yangtze Delta tended to be weaker and change directions (Fig. 4b).

3.2. Remote impacts of typhoons on coastal hydrodynamics

3.2.1. Impact on waves

During our observations of the mudflat in the Yangtze Delta, the tide-averaged significant wave height at the mudflat station was closely correlated with the tide-averaged significant wave height at the nearshore station ($R^2 = 0.56$, data shown in Table S1). Thus, the wave heights at the nearshore station prior to our mudflat observation can be used to understand the wave conditions on the mudflat for a longer time period. At the nearshore station in the Yangtze Delta front, the lowest wave heights were all found during calm weather (wind speed < 2–3 m/s). For example, at the nearshore station, where the water depth is 5 m on average, the significant wave height (6-hour average) was lowest (ca. 0.2 m) on 15 July, 4 August and 9 September (Fig. 4c). These minimal wave heights likely had little relation to tidal conditions because they were recorded under different tidal conditions ranging from neap (15 July) to spring tides (5 August) (Fig. 4). On the other hand, the highest wave heights were recorded during remote typhoons that increased the wind speed in the Yangtze Delta. Specifically, the significant wave height at the nearshore station reached 1.5 m on 28 August (T_{113}) when Typhoon Lionrock was passing more than 1500 km away with a maximum wind speed 51 m/s near the typhoon eye (Fig. 4); this wave height was 7.5 times higher than the wave height under calm weather (Fig. 4). The second largest wave height, 1.4 m, was recorded during T_{155} (September 18–19) when Typhoon Malakas was passing 450 km away with a maximum wind speed 46 m/s near the typhoon center. The third largest wave height (1.35 m) was observed during T_{173} (September 28) when Typhoon Megi was passing 770 km away with a maximum wind speed of 29 m/s near the typhoon center (Fig. 4).

Similar to the wind speed in the Yangtze Delta, the wave height at this delta was affected by only some remote typhoons and only during part of their duration. The maximum tide-averaged significant wave height during the non-typhoon periods was 0.65 m. Among the 115 tides when one or two typhoons were moving across the Pacific Ocean, 37 tides were accompanied by tide-averaged significant wave heights higher than the maximum wave height during the non-typhoon periods. The significant wave heights during these 37 tides were on average 0.9 m. The waves in the Yangtze Delta were most likely affected by remote typhoons during these 37 tides. On average, the < 0.59 m significant wave heights in the typhoon periods were equal to the significant wave heights in the no typhoon periods. Thus, the 0.59–65 m

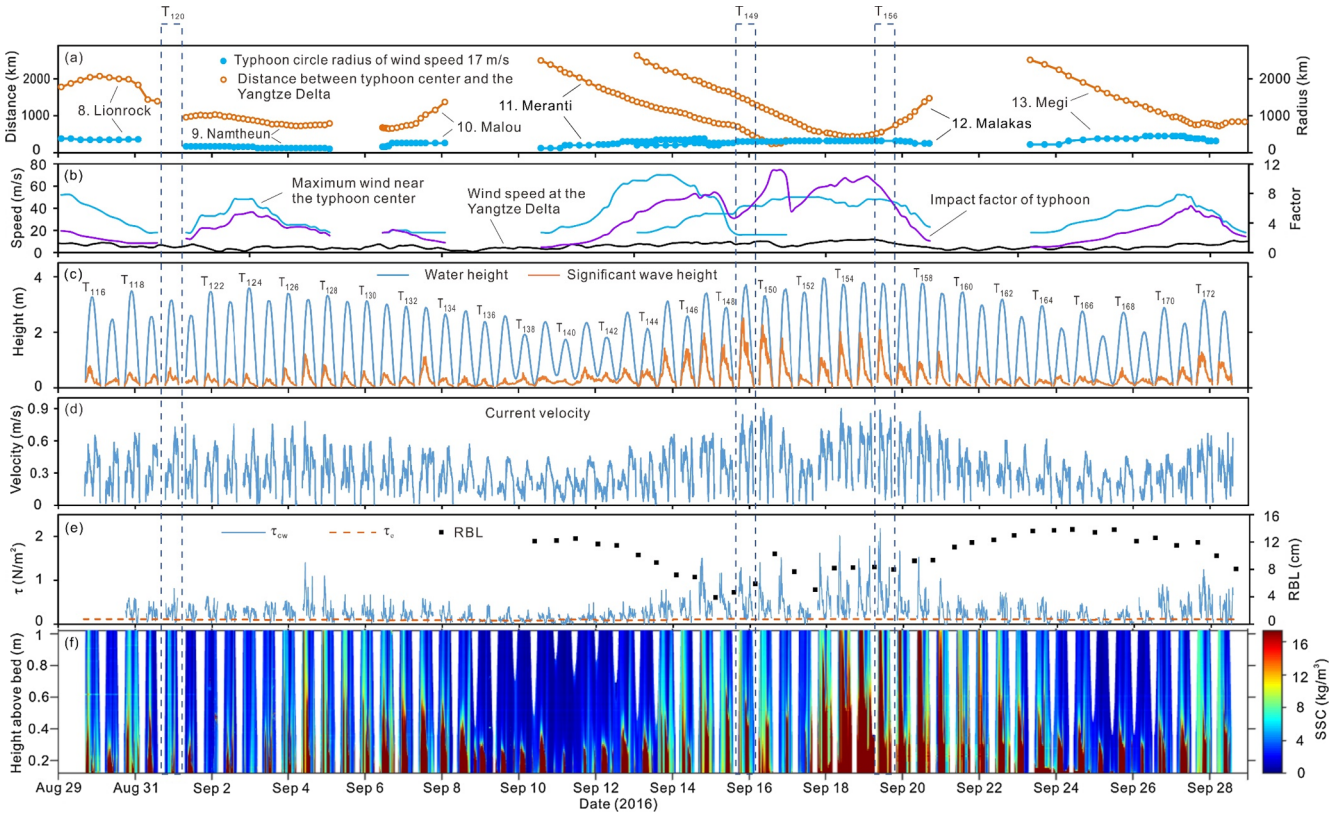

Fig. 5. Time series of remote typhoon information, wind speed at the nearshore station in the Yangtze Delta front, and hydrodynamics and suspended sediment concentration measured at the mudflat site. (a) distance between typhoon center and Yangtze Delta, and typhoon circle radius of wind speed 17 m/s, (b) maximum wind speed near the typhoon center, wind speed at the Yangtze Delta, and impact factor of typhoon, (c) water height and significant wave height at the mudflat measurement site, (d) near bed current velocity (0.5 m above bed), (e) bed shear stress due to combined current–wave action (τcw), critical shear stress for erosion of sediment (τe) and relative bed level (RBL) changes, (f) suspended sediment concentration (SSC) profiles (Enlarged comparisons between T120, T149, T156 are shown in Figs. 7 and 8).

significant wave heights in the typhoon periods may also have been influenced by typhoons. These significant wave heights were observed during 12 tides (Table S1). Therefore, we concluded that the significant wave heights were influenced to different extents by typhoons during 49 tides, or 43% of the duration of the typhoon periods. Thus, the number of tides associated with a detectable typhoon impact on waves in the Yangtze Delta was much greater than the number of tides associated with a detectable typhoon impact on wind speed. This result suggests that the impacts of remote typhoons on waves in the Yangtze Delta included not only an increase in wind-driven waves in the delta itself but also swells that propagated into the Yangtze Delta area from the remote Pacific Ocean where one or more typhoons generated tall waves. Thus, even if the winds in the Yangtze Delta are not affected by a remote typhoon, the waves generated by this typhoon in the far ocean may partly propagate into waters near the Yangtze Delta.

For typical typhoon events that significantly influenced the waves in the Yangtze Delta, the wave height in the Yangtze Delta nearshore station (H_N) was closely correlated with the impact factor of the typhoon. For example, the correlation coefficient R^2 between H_N and IF_T reached 0.94 (significance level $p < 0.05$) during Typhoon Malakas (Fig. S2a). For Typhoon Meranti, when a 0.5 day (1 tide) lag in wave height was considered, the correlation coefficient between H_N and IF_T reached its peak ($R^2 = 0.58, p < 0.05$) (Fig. S2b). A similar time lag in wave height in the Yangtze Delta after the impact factor of typhoon was also observed during Typhoon Lionrock. For this typhoon, when a 2-day (4-tide) lag in wave height was considered, the correlation coefficient between H_N and IF_T was at its highest ($R^2 = 0.82, p < 0.01$) (Fig. S2-c). For all the impacting typhoons, defined as the periods when a typhoon impact on wave height in the Yangtze Delta was detected, the correlation coefficient between H_N and IF_T reached its maximum at $R^2 = 0.43$ ($p < 0.001$), when a 0.5 day lag in wave height was considered (Fig. S2-d). In contrast, for the non-impacting typhoons that did not affect the Yangtze Delta, the correlation coefficient between H_N and IF_T decreased to only $R^2 = 0.07$ (data shown in Table S1).

The time lag of H_N after IF_T was presumably relevant to the progradation of the swells across the open Pacific. For example, the distance between the Yangtze Delta and the storm center was on average 1600 km during Typhoon Lionrock. Based on Equation (2), the period of waves travelling across the 1600 km distance over 2 days would be ca.12 s, which is supported by the wave periods in the western Pacific during the Typhoon Lionrock predicted by the European Centre for Medium-Range Weather Forecasts (ranging from 11 to 15 s, and being 12.1 s on average). Although the origin and progradation of waves on the open ocean could be more complex than addressed above, our coarse estimation likely explains the main mechanism of the time lag among the waves in the Yangtze Delta after a remote typhoon occurrence.

During the impacting typhoons, the distance between the typhoon center and the Yangtze Delta, the maximum wind speed near the typhoon center, the impact factor of typhoon and the significant wave height at the nearshore station in the Yangtze Delta were on average 1600 km, 38 m/s, 4.3 and 0.85 m, respectively. During the non-impacting typhoons, they were on average 2100 km, 27 m/s, 1.9 and 0.42 m (equal to the mean significant wave height under no typhoon weathers), respectively.

At the mudflat station, the tide-averaged significant wave height was positively correlated with the tide-averaged water depth during the periods of no typhoon, non-impacting typhoon and impacting typhoon.

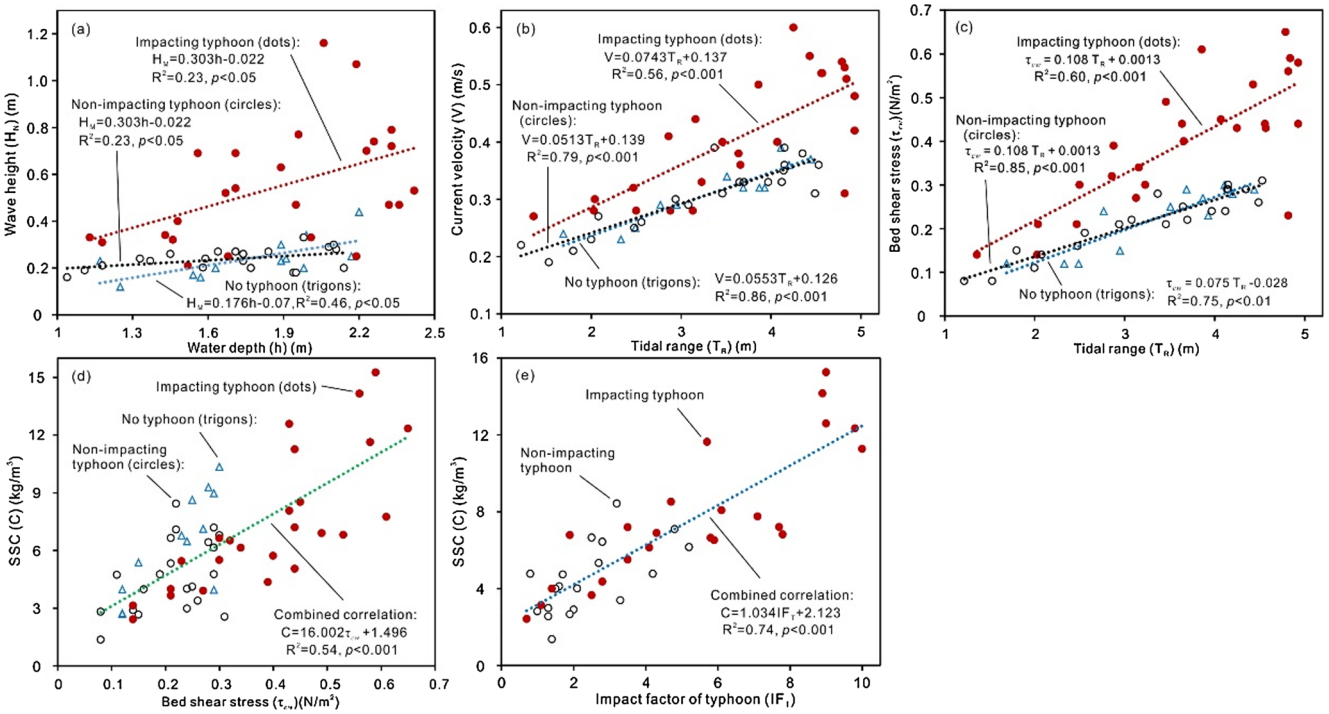

Fig. 6. The typhoon impacts on hydrodynamics and SSC reflected by scatter diagrams of variables under conditions of an impacting typhoon, non-impacting typhoon and no typhoon. (a) The correlations between the tide-averaged significant wave height and tide-averaged water depth measured at the mudflat station. (b) The correlations between the tide-averaged near-bed current velocity measured at the mudflat station and astronomical tidal range. (c) The correlations between the tide-averaged bed shear stress due to combined current-wave action and astronomical tidal range. (d) The correlation between tide-averaged SSC and tide-averaged bed shear stress. (e) The correlation between the tide-averaged SSC and tide-averaged impact factor of typhoon with a 2-tide lag of the SSC behind the impact factor of typhoon (for the non-impacting typhoon category, $C = 0.695\ IF_T + 2.311$, $R^2 = 0.36$, $p = 0.032$) (original data shown in Table S1). "Impacting typhoon" represents the periods when the impacts of remote typhoons on the Yangtze Delta were detected. "Non-impacting typhoon" represents the periods when the impacts of remote typhoons on the Yangtze Delta were undetected. "No typhoon" represents the periods when no typhoon occurred.

The correlation between wave height and water depth under no typhoon was similar to that under non-impacting typhoon. However, the correlation trendline of the impacting typhoon was far above the correlation trendlines of the no typhoon and non-impacting typhoon (Fig. 6a), suggesting that the wave height during impacting typhoons were substantially higher than the wave heights during no typhoon and non-impacting typhoon periods at equal water depths. Based on the correlation equations, the wave heights under the impacting typhoons (0.55 m) were on average 2.2 times higher than the wave heights under no typhoon and non-impacting typhoon conditions (0.25 m). The maximum typhoon impact on wave height occurred during the twin Meranti and Malakas Typhoons when the tide-averaged significant wave height measured at the mudflat station reached 1.16 m during tidal cycle T_{150} (Fig. 5 and Table S1), which was 4.2 times higher than that (0.28 m) predicted by the correlations for non-impacting typhoon and no typhoon situations in Fig. 6a (for 2.06 m of water depth in tidal cycle T_{150}). Considering that the tide-averaged water depth over the mudflat is mainly determined by tidal range, the correlation between tide-averaged wave height and water depth basically reflects the tide control.

The wave height measured at the mudflat station tended to show peak values in the flood phase of each tidal cycle (Fig. 5c). The asymmetry in the intra-tidal wave height curve likely reflects the difference in influencing factors between the flood and ebb phases. During the flood phase, the wave propagation direction was the same as the onshore tidal current direction. On the other hand, during the ebb phase, the wave propagation direction was opposite the offshore tidal current direction. The intra-tidal pattern of wave height (i.e., increasing in the flood phase and decreasing in the ebb phase) also reflects the strong influence of water depth on waves in tidal wetlands (Yang et al., 2012). This intra-tidal pattern was present because of the high resolution of the wave measurements, i.e., 10-min average. If the resolution of wave height was 6 h, as at the nearshore station, then the above intra-tidal pattern could not be observed. Despite the intra-tidal pattern of wave height, the impact of typhoons on wave height in the Yangtze Delta was clearly detectable. In addition to the statistical result for the impacting typhoons as a whole (Fig. 6a), typhoon impacts were also reflected in individual typhoon events. Specifically, the wave heights during the Twin Typhoons Meranti and Malakas and Typhoon Megi were significantly higher than in other impacting typhoon periods. The comparison of the intra-tidal wave height curve between two typical tidal cycles, T_{120} and T_{149}, which were equal in tidal range (4.44 *vs* 4.43 m) and high tide height (5.20 *vs* 5.17 m) but were different in weather condition (No typhoon *vs* Twin Typhoons Meranti and Malakas) (Fig. 5, Table S1), strikingly shows the storm impact on waves at the Yangtze Delta (Fig. 7c). During the non-typhoon tidal cycle T_{120}, the mean wind speed at the Yangtze Delta was 5.31 m/s, and the mean significant wave heights at the nearshore and mudflat stations were 0.46 and 0.34 m, respectively. In contrast, during the typhoon-affected tidal cycle T_{149}, the mean wind speed was 8.44 m/s, and the mean significant wave heights at the nearshore and mudflat stations were 0.87 and 1.07 m, respectively (Fig. 5 and Table S1). The intra-tidal maximum wave height at the mudflat station was 0.72 m in T_{120} and 2.50 m in T_{149} (Fig. 5c).

3.2.2. *Impact on currents*

Tidal current velocity increases with tidal range (Alvarez, 2010; Call et al., 2015). This scenario is supported by our finding that the tide-averaged near-bed current velocity at the mudflat station was closely correlated with the astronomical tide range (Fig. 6b). However, the correlation trendline of the impacting typhoon situation was significantly above the correlation trendlines of the non-impacting

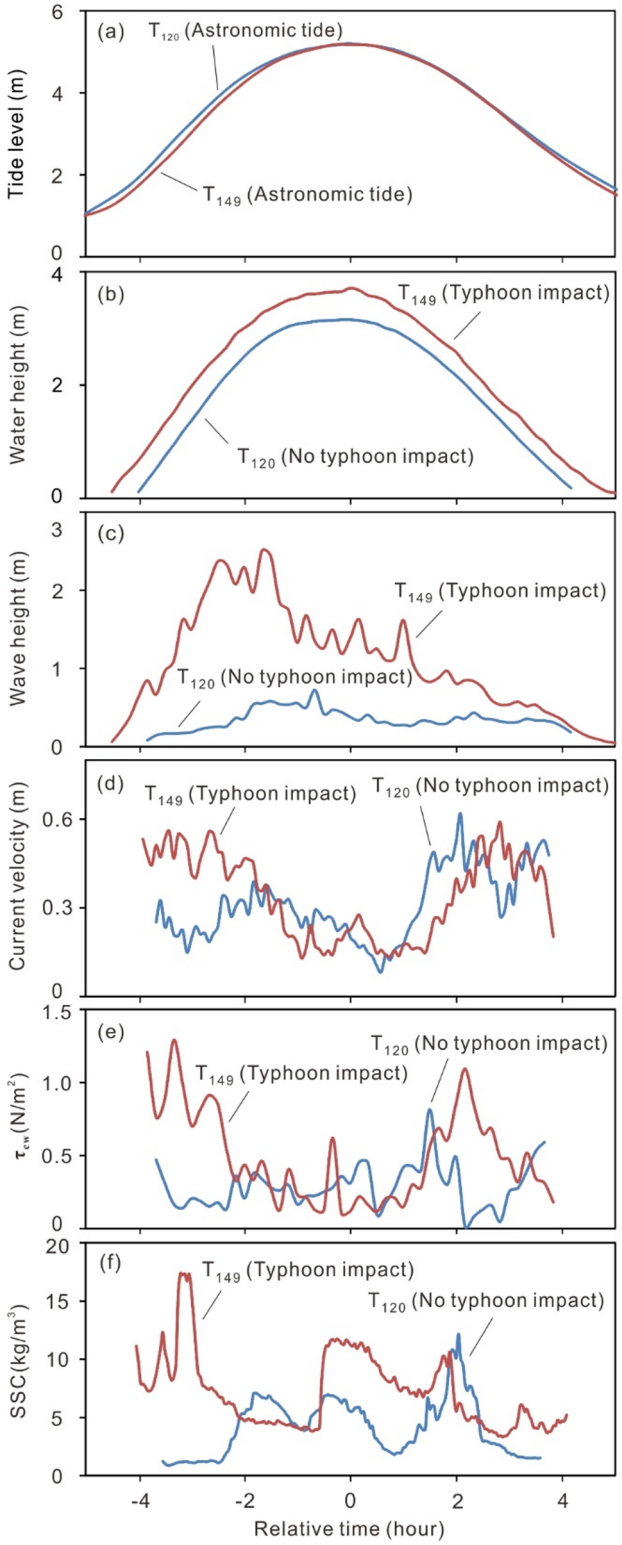

Fig. 7. An example of typhoon-generated overall increases in intra-tidal water height/submergence duration, wave height, current velocity, bed shear stress due to combined current-wave action (τ_{cw}) and suspended sediment concentration (SSC), reflected by comparison between two similar astronomical tides (T_{120} and T_{149} indicate the orders of the two astronomical tides. The astronomical tide range was 4.44 m during T_{120} and 4.43 m during T_{149}, whereas the wind speed was 5.31 m/s during T_{120} and 8.44 m/s during T_{149}. The intra-tidal series of the typhoon parameters and the wind speed in the Yangtze Delta, and the comparison between T_{120} and T_{149} and other tidal cycles are shown in Fig. 5).

typhoon and no typhoon situations, whereas the correlation trendlines of the non-impacting typhoon and no typhoon situations were similar. This result suggests that given the same tidal range the current velocity during impacting typhoons was significantly higher than the current velocity during non-impacting typhoons and no-typhoon periods. Based on the correlation equations, the current velocities during the impacting typhoons (0.41 m/s) were on average 24% higher than the current velocities during the non-impacting typhoon and no-typhoon periods (0.33 m/s). The maximum typhoon impact on current velocity occurred during the twin Typhoons Meranti and Malakas when the tide-averaged current velocity measured at the mudflat station reached 0.6 m/s (Tidal cycle T_{150}) (Fig. 5 and Table S1), which was 67% greater than that (0.36 m/s) predicted by the correlations for the non-impacting typhoon and no typhoon situations in Fig. 6b (for 4.25 m of tidal range during tidal cycle T_{150}). Strikingly, the maximum typhoon impact on current velocity occurred at the same time as the maximum typhoon impact on wave height, i.e., on September 16 (T_{150}) (Fig. 5 and Table S1).

The typhoon impact on current velocity in the intertidal wetland was also reflected in the comparison of intra-tidal velocity curves between two tides that were equal in astronomical tidal ranges but were different in wind speeds and wave heights. For example, during the two tidal cycles of T_{120} and T_{149}, the astronomical tidal ranges were 4.44 and 4.43 m, and the wind speeds were 5.31 and 8.44 m/s, respectively (Table S1). During these two tides, the overall v-shaped intra-tidal pattern of the velocity curves hardly changed. That is, the velocity decreased during the flood phase, reached a minimum approximately at the high tide, and then increased during the ebb phase. However, the current velocity of T_{149} was generally higher than the velocity of T_{120}. The increased velocity occurred mainly in the earlier (or shallower) flood stage (Fig. 7d). On average, the current velocity was 0.37 m/s during tide T_{120} and 0.55 m/s during tide T_{149}, corresponding to a significant wave height of 0.34 m in T_{120} and 1.07 m in T_{149} (Table S1).

The overall increase in current velocity due to a typhoon impact was attributable to wind-induced currents (Wu, 1975; Weber, 1983; Chang et al., 2012) and wave-induced flow (Shaikh and Siddiqui, 2011). The wind- and wave-induced near-bed currents are assumed to be inversely proportional to water depth and to be significant in shallow waters such as that over the intertidal wetland. The correlation coefficient between current velocity and tidal range was relatively lower under a typhoon impact ($R^2 = 0.56$) than under conditions of a non-impacting typhoon and no typhoon ($R^2 = 0.75$–0.79) (Fig. 6b). This result likely reflects that the superposition of typhoon-induced currents, which are independent of tidal range, somewhat disturbs the relationship between current velocity and tidal range. Furthermore, the storm-induced currents observed during this study likely varied among the typhoon events.

3.2.3. Impact on bed shear stress

As an indicator of combined current-wave action for estimating sediment pick-up rate, τ_{cw} measured on the mudflat showed spring-neap and storm-no storm patterns similar to current velocity and wave height (Fig. 5). The change in τ_{cw} was the comprehensive impact of tidal variation, local winds and typhoons. Like the tide-averaged wave height and current velocity, the tide-averaged τ_{cw} was closely correlated with the tidal range. However, the correlation trendline of the impacting typhoon category was far above the correlation trendlines of the non-impacting typhoon and no typhoon categories. Based on the equations of these correlations, the τ_{cw} values under the impacting typhoons were on average 0.40 N/m^2, or 60% higher than the mean τ_{cw} value (0.25 N/m^2) predicted for the no typhoon and non-impacting typhoon conditions. The maximum typhoon impact on tide-averaged τ_{cw} was also occurred during the twin typhoons Meranti and Malakas. The measured τ_{cw} in the tidal cycle T_{147} was 0.61 N/m^2, which was 2.3 times higher than the 0.26 N/m^2 predicted for the non-impacting typhoon and no typhoon situations using the correlations in Fig. 6c, given the 3.86 m in

tidal range). That the time of the maximum typhoon impact on τ_{cw} slightly deviated from the time of the maximum typhoon impacts on wave height and current velocity is probably because the τ_{cw} is determined by not only wave height and current velocity but also water depth and velocity profile (Whitehouse et al., 2000).

The comparison of τ_{cw} between T_{120} and T_{149} that are equal in tidal condition was most convincing for the typhoon impact during an individual tidal cycle. The average τ_{cw} was 0.29 N/m^2 during the no-typhoon tide T_{120} and 0.53 N/m^2 during the stormy tide T_{149}. The intra-tidal patterns of τ_{cw} in the two tides were similar, but τ_{cw} during T_{149} was significantly greater than during T_{120} for most of the tidal cycle (Fig. 7e). Under no-typhoon and neap tidal conditions, τ_{cw} was close to the critical shear stress for erosion (τ_e). For example, during the no–typhoon neap tide T_{136}, the τ_{cw} ranged from 0.01 to 0.45 and 0.12 N/m^2 on average, in comparison with τ_e (0.09 N/m^2). This suggests that bottom sediment can be resuspended only in part of the tide duration in the period of calm weather and neap tides. However, during typhoon-affected tidal cycles (e.g., $T_{147}-T_{151}$, $T_{153}-T_{156}$), all τ_{cw} values could be greater than τ_e, and the averaged τ_{cw} could be 5 times higher than τ_e.

In addition, the water height and submergence duration on the intertidal wetland increased during 80% of the storm-affected tidal cycles. For example, the water height at the high tide of T_{149} increased by 0.15 m, and the submergence duration on the intertidal wetland lengthened by 0.25 h (Fig. 6b). The maximum increases in water height and submergence were 0.43 m and 0.7 h, respectively.

3.3. Remote impact of typhoons on coastal suspended sediment concentration

The SSC measured in the 1 m water column above the mudflat in the Yangtze Delta showed a similar temporal pattern to that of τ_{cw} (Fig. 5). There was a significant positive correlation between the tide-averaged SSC and tide-averaged τ_{cw} (Fig. 6d). However, the highest τ_{cw} ~ SSC data couples were measured during the impacting typhoons, whereas no significant difference between non-impacting typhoons and no typhoons was found (Fig. 6d). Based on the correlation shown in Fig. 6d, the SSC would be 7.9 kg/m^3 for the mean τ_{cw} of impacting typhoon (0.40 N/m^2), and would be 5.5 kg/m^3 for the mean τ_{cw} of non-impacting typhoon and no typhoon (0.25 N/m^2), suggesting that the SSC was increased by 44% on average by the typhoon impacts. Similarly, the SSC would be 11.3 kg/m^3 during the tidal cycle T_{147} when the typhoon impact on τ_{cw} reached its maximum (0.61 N/m^2), and would be 5.7 kg/m^3 for the corresponding τ_{cw} under presumed non-impacting typhoon and no typhoon conditions (0.26 N/m^2), suggesting that the tide-averaged SSC during the maximum impacting typhoon was 2.0 times greater than the SSC under non-impacting typhoon and no typhoon situations. That is, some of the remote typhoons significantly increased the SSC in the intertidal wetland of the Yangtze Delta by affecting the delta hydrodynamics.

In the classic comparison between two tides that are equal in tidal range and high tidal level, the SSC in the typhoon-influenced tide T_{149} (6.81 kg/m^3) was 1.7 times higher on average than the SSC in the no-typhoon tide T_{120} (3.94 kg/m^3), although the intra-tidal and vertical patterns of SSC in the two tidal cycles were similar (Fig. 7f; Fig. 8). During the typhoon-affected tides T_{153}–T_{158}, when the difference between τ_{cw} and τ_e becomes greater than during tide T_{149} (Fig. 5f, Table S1), the tide-averaged SSCs reached 11.6–15.3 kg/m^3 (Table S1), suggesting that the amount of resuspended sediment is proportional to the difference between τ_{cw} and τ_e. During these tides, the SSC in several decimeters closest to the bottom even exceeded the upper detection limit of ASM (17.3 kg/m^3) (Fig. 8). It is necessary to indicate that the tidal cycles of T_{153}–T_{158} were spring tides (Fig. 5). The extremely high SSCs during this period reflect the combined impact of typhoon and spring tides. The tidal ranges of the tidal cycles T_{153}–T_{158} were 4.75 m on average. According to the correlations between tidal range and τ_{cw} under the non-impacting typhoon and no typhoon conditions (Fig. 6c),

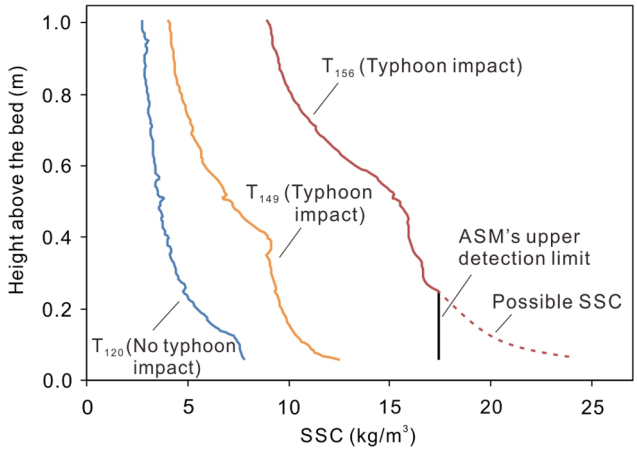

Fig. 8. Examples of typhoon-generated increase in SSC profile (each profile was tide-averaged and was measured by ASM within the 1-m near-bed water column. The astronomical tide range was 4.44 m during T120, 4.43 m during T149 and 4.79 m during T156, whereas the wind speed was 5.31 m/s during T120, 8.44 m/s during T149, and 10.20 m/s during T156). See Appendix B for more details.

the τ_{cw} would be 0.32 N/m^2, given the tidal range 4.75. This τ_{cw} value would result in an SSC of 6.6 kg/m^3, based on the correlation between SSC and τ_{cw} (Fig. 6d). The long-term average tidal range in the study area is 3.2 m (Zhu et al., 2014), which would result in a τ_{cw} of 0.21 N/m^2 and an SSC of 4.9 kg/m^3 under non-impacting typhoon and no typhoon conditions, based on the correlations in Fig. 6c and d. The SSCs observed during T_{153}–T_{158} were on average 12.9 kg/m^3 (Table S1). Thus, compared with the SSC under normal weather and tidal conditions, the SSC increased by 8.0 kg/m^3 during the stormy and spring tidal period of T_{153}–T_{158}. 21% of this rise in SSC was attributed to increased tidal range, whereas 79% of the rise in SSC was due to the impact of the remote typhoon (Malakas).

The SSC in the Yangtze Delta was closely correlated with the impact factor of the typhoon. With a 2 tide lag in SSC after IF_T was considered, the correlation coefficient reached the maximum $R^2 = 0.74$ ($p < 0.001$) (Fig. 6e) that was significantly greater than the in-phase correlation coefficient between the SSC and IF_T ($R^2 = 0.36$, $p < 0.001$). For the non-impacting typhoon category alone, the in-phase correlation between the SSC and IF_T was not statistically significant ($R^2 = 0.01$, $p = 0.92$, correlation diagrams omitted), even though the 2 tide lag correlation became closer (Fig. 6e). This suggests that the above significant correlation between the SSC and IF_T was contributed mainly by the data of impacting typhoon. Based on Fig. 6e, we conclude: 1) When $IF_T > 5.2$, the remote typhoon was certainly an impacting typhoon that would cause sediment resuspension and increase SSC in the Yangtze Delta; 2) When $IF_T < 5.2$, the remote typhoon could be either an impacting typhoon or a non-impacting typhoon. Considering that the SSC was also influenced by tidal range, we established a binary regression relationship to reflect the combined influences of typhoon and tidal range:

$$\text{in}-\text{phase correlation: } C = 1.629\,T_R + 0.428\,IF_T - -1.045,\ R^2 = 0.57,\ p < 0.001 \quad (3)$$

$$2-\text{tide C lag behind } IF_T\text{: } C = 0.654\,T_R + 0.929\,IF_T + 0.262,\ R^2 = 0.79,\ p < 0.001 \quad (4)$$

where C represents the SSC (kg/m^3), T_R represents the tidal range. These binary regressions suggest that, as an SSC lag was considered, 1) the correlation coefficient significantly increased, 2) the module reflecting the weight of IF_T increased (from 0.428 to 0.929), whereas the module reflecting the weight of T_R decreased (from 1.629 to 0.654). The SSC lag presumedly resulted from the hydrodynamics lag after the

remote impacting typhoon as shown above. Thus, it is necessary to consider a time lag in studying the impact of remote typhoon on sediment resuspension and bed stability.

The time duration of storm impact on SSC is likely longer than the impact on hydrodynamics because the deposition of suspended fine-grained sediments after the decline of hydrodynamics in the post-storm period requires some time. This time lag of SSC decline was well shown in the post-Malakas period. For example, during tides T_{159}–T_{162} after Typhoon Malakas, the SSC was 8.6–10.3 kg/m^3, much higher than usual, although the hydrodynamics had decreased to a very low level (Fig. 5; Table S1). It is also due to this time lag that the SSC during mean tides after spring tides tends to be higher than the SSC during mean tides prior to spring tides, given similar weather conditions (Osborne and Greenwood, 2010).

3.4. Remote impact of typhoons on seabed stability

In previous studies, it was found that typhoon or hurricane landfall tends to cause severe erosion in the subtidal seabed, mudflat and low marsh edges, whereas it causes rapid accretion in the inner marsh area (Yang et al., 2003; Turner et al., 2006). In the present study, after the passing of a series of remote typhoons, net erosion was found on the mudflat, even though deposition was observed somewhere. The comparison between the cross-shore intertidal wetland profiles surveyed before and after the typhoons suggests that most of the mudflat experienced erosion during the typhoon season. The net erosion in the mudflat profile was 3 cm, and the maximum erosion reached 22 cm in the transitional zone between the mudflat and the marsh. Deposition was found only in the middle flat where the sediment surface was originally low-lying (Fig. 9). At the tripod system observation site, the erosion during the Twin Meranti and Malakas typhoons reached a maximum of ca. 8 cm (Fig. 5e).

After the Twin Meranti and Malakas typhoons, the mudflat experienced a week of deposition and bed-level recovery (Fig. 5e). In a previous study of typhoon impact on intertidal wetland stability in the Yangtze Delta, the bed-level recovery period was also found to be approximately a week (Yang et al., 2003). Nevertheless, the one week of bed-level recovery coincided with a transition period from spring to neap tides both in the present and the previous study. Presumedly, the SSC tends to decrease from spring to neap tides, and the mudflat tends to experience deposition and bed-level recovery, unless this process is interrupted by storm events. Thus, the bed-level recovery period would be longer than a week under other conditions (e.g., transition from neap to spring tides), given the same storm-generated erosion as found in this study.

The temporal trend of the relative bed level is overall opposite to that of the τ_{cw} on the mudflat (Fig. 5e), and the correlation coefficient (R) between these variables is 0.6. This suggests that the mudflat tends to erode as the τ_{cw} increases, and vice versa. As shown above, although the increase in τ_{cw} during the Twin Typhoons was partly owing to the spring tides, the impact from the typhoons was obvious. Therefore, the erosion on the mudflat should be partly attributed to typhoons. Considering that the changes in SSC in the mudflat are the results of sediment deposition/pick-up, and that sediment deposition/pick-up are directly link with bed-level changes, the significant increase in SSC during typhoon events also suggests strong seabed erosion.

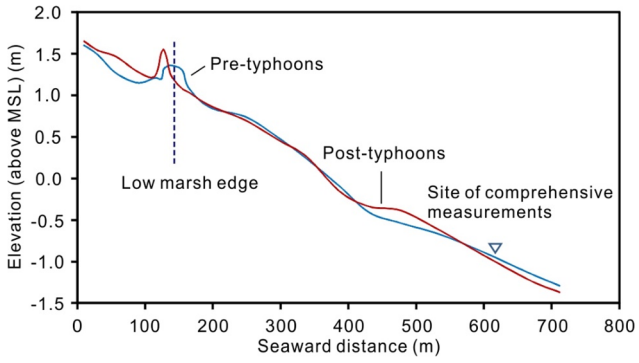

Fig. 9. Cross-shore intertidal wetland profiles surveyed before and after the typhoons (MSL: mean sea level. The pre-typhoons and post-typhoons were surveyed on July 10 and September 19, 2016).

During the same period, we also found an erosion of 12 cm at the low marsh edge. However, most of the marshes experienced deposition. The mean marsh deposition in the cross-shore profile was 13 cm (Fig. 9). Noticeably, we found the formation of a washover sand body in the low marsh, which buried the existing plant (*Scirpus mariqueter*) and silted up a tidal creek (Fig. 10). The comparison between the pre- and post-typhoons profiles suggests that the formation of this washover sand likely linked with the landward movement of an earlier washover sand body, and the maximum deposition in the center of the present washover sand body reached 31 cm (Fig. 9). The washover sand body was composed of fine sands (median size d_{50} = 0.13–0.16 mm), which are much coarser than the mud found both on the mudflat (d_{50} = 0.04–0.06 mm) and on the inner marsh (d_{50} = 0.007–0.024 mm). The elevation of the washover sand body was 10–30 cm higher than the marshland on the landward side. Excavating the sand cover, residual stems of the marsh plant were exposed, suggesting that the washover sand body was rapid deposition on the marsh. We infer that the washover sand body was formed during typhoon storm surges. We found that under non-typhoon conditions, waves were low and currents were weak near the high tide, which were unfavourable conditions for the movement of sands as bed load, leading to only mud deposition in this area. In contrast, during typhoon storm surges, extremely large and high waves hit the low marsh edge, leading to strong wash flows, which eroded the mud and left sands. As a result, a washover sand body was formed on the landward side of the low marsh edge. Storm-generated washover sand bodies were often found in backbarrier marshes (Donnelly et al., 2004). On other coasts of the Yangtze Delta, washover sand deposits were also formed in low salt marshes during the landfalls of strong typhoons (Yang et al., 2000, 2003). In the present study, we found that large washover sand bodies also developed in low salt marshes during storm surges even if the typhoons were passing hundreds of kilometers away. The different morphological responses to typhoons between the marsh and the mudflat also increased the elevation gradient in the mudflat-marsh transitional zone (Leonardi et al., 2018).

3.5. Determinants of remote typhoon impacts

Our results suggest that the Yangtze Delta was affected by only some of the remote typhoons and during only part of the impacting typhoons. The impact of a typhoon on an intertidal wetland is presumedly determined by the integration of multiple factors, such as typhoon strength, distance between a typhoon and the coast, typhoon duration, marine bathymetry, coastal configuration, sediment composition of the intertidal wetland, marsh/swamp vegetation, tidal conditions (e.g., microtidal, mesotidal or macrotidal; spring or neap tides), and previous state of erosion/accretion. The typhoons that did not affect the Yangtze Delta were too far away or/and relatively weak. Specifically, Typhoon Lupit had maximum wind speeds of only 18 m/s near the storm center and was more than 3400 km away from the Yangtze Delta, Typhoon Nida had maximum wind speeds of 18–38 m/s and was 1200–1600 km away, Typhoon Conson had maximum wind speeds of 20–27 m/s and was 3200–3700 km away, and Typhoon Chanthu had maximum wind speeds of 18–23 m/s and was 1900–3200 km away. Our attempt to use the IF_T factor to quantify the remote impact of typhoons was not perfect because it only reflects the impact of typhoon strength and the distance between the typhoon center and the studied coast (Eq. (1)). This approach fails to incorporate the impacts of other influencing factors. As a

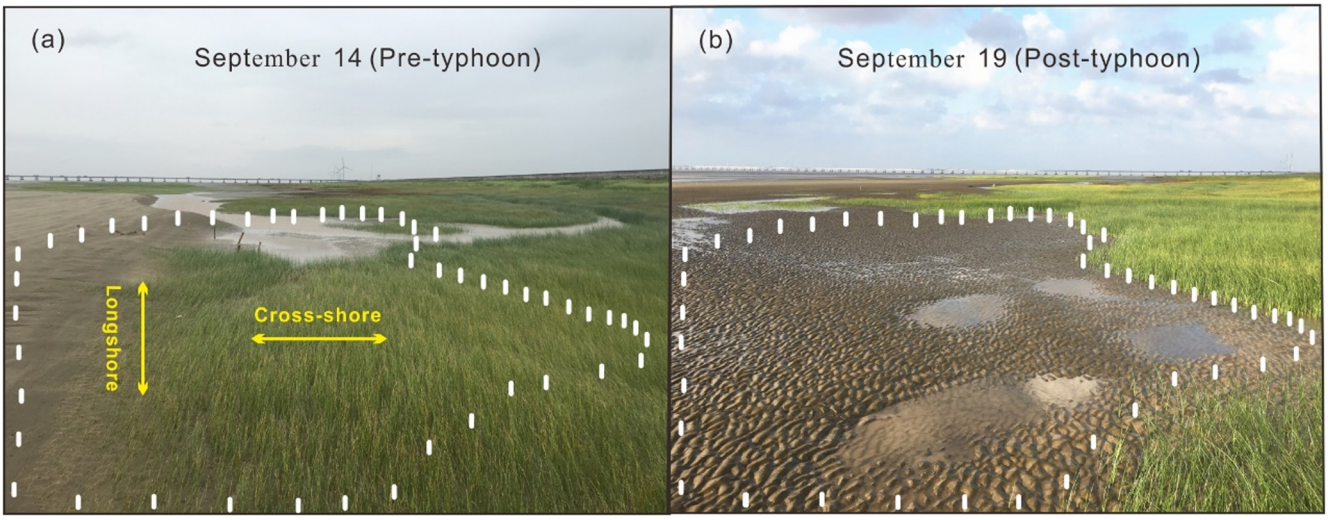

Fig. 10. Typhoon-generated washover fine-sand body which buried the existing plant and silted up a tidal creek in the low marsh (The white bars in the two panels delineate the same area which is 7 m in the cross-shore direction and 50 m in the longshore direction).

result, the correlations between IF_T and coastal wind speed/wave height were not close when all typhoon events were considered ($R^2 < 0.45$), although the R^2 could exceed 0.95 for individual typhoons (Fig. S1, Fig. S2). When the IF_T was higher than 5.2, the intertidal wetlands in the Yangtze Delta was clearly affected by the remote typhoon. However, when the IF_T ws lower than 5.2, the intertidal wetlands in the Yangtze Delta could be impacted or could not be impacted by the remote typhoon, depending on the influenced of other factors. Considering the shortcomings of the IF_T shown above, more influencing factors need to be incorporated into this impact factor in future studies to improve its accuracy and applicability.

4. Conclusions

The intertidal wetland in the Yangtze Delta was influenced to different extents by 8 of the 13 typhoons that occurred in the west Pacific Ocean during July through September 2016. The delta was affected during half of the duration of these 8 typhoons. During the influenced periods, the distance between the delta and the typhoon center was 450–2000 km, and the maximum wind speed near the typhoon center was 20–62 m/s. The typhoons that did not affect the Yangtze Delta were too far (> 2000 km from the delta) or/and relatively weak (< 20 m/s in maximum wind speed near the storm center). The typhoons impacting the delta increased wind speed (11.5 m/s with maximum impact *vs* 4.8 m/s on average with no storm impact), water height (3.73 m *vs* 3.30 m), duration of tidal inundation (8.8 h *vs* 8.1 h), wave height (1.2 m *vs* 0.26 m) and current velocity (0.60 m/s *vs* 0.31 m/s), thereby enhancing the bed shear stress due to combined current-wave action (0.65 N/m^2 *vs* 0.27 N/m^2) and resulting in sediment suspension (15.3 kg/m^3 *vs* 4.5 kg/m^3 in near-bed SSC). During the periods of impacting typhoons, the mudflat experienced considerable net erosion, whereas the main marsh experience rapid deposition and the low marsh was buried by a washover fine-sand body, and a creek there was silted up. We conclude that the hydrodynamic, sedimentary and erosion/accretion processes in intertidal wetlands can be significantly influenced by typhoons even if they pass hundreds of kilometers or more than a thousand kilometers away. These findings contribute to increase knowledge of how far and in what extent hurricanes/typhoons can affect intertidal wetlands that is needed for coastal management strategy.

5. Data accessibility

The data of typhoon tracks and maximum wind speeds near the typhoon centers are available at http://www.nmc.cn/; the data of wind speeds and wave heights at the nearshore station in the Yangtze Delta are available at https://www.ecmwf.int/. The data of tide-averaged values of the factors are shown in Table S1. For other data, please contact Fan, J. (719735027@qq.com).

Declaration of Competing Interest

The authors declare that they have no known competing financial interests or personal relationships that could have appeared to influence the work reported in this paper.

The authors declare the following financial interests/personal relationships which may be considered as potential competing interests:

Acknowledgments

We thank Tian Yang, Haobin Wang, Wenxiang Zhang and Weiwei Qian for their assistance in the fieldwork. This study was funded by the Natural Science Foundation of China (NSFC) (41576092), NSFC-Shandong Joint Fund for Marine Science Research Centers (U1606401), the Ministry of Science and Technology of China (2016YFE0133700), and the Royal Netherlands Academy of Arts and Sciences (PSA-SA-E-02).

Appendix. A. The calculation of bed shear stress

The bed shear stress due to waves (τ_w, N/m^2) can be expressed as follows (Van Rijn, 1993):

$$\tau_w = \frac{1}{2}\rho_w f_w \hat{U}_\delta^2 \quad (A1)$$

where $\rho_w$is the seawater density (=1028 kg/m^3), and $\hat{U}_\delta$and$f_w$are the peak orbital velocity and wave friction coefficient, respectively. The peak orbital velocity $\hat{U}_\delta$ can be calculated by

$$\hat{U}_\delta = \omega \hat{A}_\delta = \frac{\pi H}{T \sinh\left(\frac{2\pi}{L}h\right)} \tag{A2}$$

$$\hat{A}_\delta = \frac{H}{2\sinh\left(\frac{2\pi}{L}h\right)} \tag{A3}$$

where ω is the angular velocity ($=\frac{2\pi}{T}$, s^{-1}), $\hat{A}_\delta$ is the peak orbital excursion, H is the significant wave height (m), T is the wave period (s), sinh is the hyperbolic sine, L is the wavelength ($=(gT^2/2\pi)\tanh(2\pi h/L)$), and h is water depth (m).

The wave friction coefficient f_w is calculated using Eq. (A4) (Soulsby, 1997):

$$f_w = \begin{cases} 2\mathrm{Re}_w^{-0.5}, & \mathrm{Re}_w \leqslant 5\times 10^5 \text{(laminar)} \\ 0.0521\mathrm{Re}_w^{-0.187}, & \mathrm{Re}_w > 5\times 10^5 \text{(smooth turbulent)} \\ 0.237 r^{-0.52}, & \text{(rough turbulent)} \end{cases} \tag{A4}$$

where $\mathrm{Re}_w = \frac{\hat{U}_\delta \hat{A}_\delta}{v}$ is the wave Reynolds number, $r = \frac{\hat{A}_\delta}{k_s}$ is the relative roughness, k_s ($=2.5\ d_{50}$) is the Nikuradse roughness (d_{50} is the median grain size of bed sediment) (Fredsøe, 1984), and v is the kinematic viscosity of water ($=1.36\times 10^{-6}\ m^2/s$).

The bed shear stress due to currents (τ_c, N/m^2) is given by (Whitehouse et al., 2000):

$$\tau_c = \rho_w u_{*c}^3 \tag{A5}$$

$$u_c(z) = \frac{u_{*c}}{\kappa}\ln\left(\frac{z}{z_0}\right) \tag{A6}$$

where ρ_w is the seawater density ($=1028\ kg/m^3$), u_{*c} is the shear velocity (m/s), $u_c(z)$ (m/s) is the current velocity at the elevation z above the bed, where z = 0.7 + RBL (0.7 m is the initial distance between the HR–Profiler' probe and the sediment surface measured prior to the first tidal inundation, and RBL (m) is the bed-level change relative to the initial sediment surface (measured by the buried-plate method), κ is Von Karman's constant ($=0.4$), and z_0 is the bed roughness length. According to the logarithmic velocity profile law, the near-bed current profiles ($u_c(z)$) collected from the HR–Profiler instrument were regressed against ln(z) using the least-squares method (Zhu et al., 2016). The $u_{*c}$was subsequently obtained on this gradient of regression line, and ultimately the τ_c was calculated according to Eq. (A5).

The bed shear stress due to waves and currents (τ_{cw}, N/m^2) during the 10-min periods is calculated as (Soulsby, 1995):

$$\tau_{cw} = \tau_c\left[1 + 1.2\left(\frac{\tau_w}{\tau_c + \tau_w}\right)^{3.2}\right] \tag{A7}$$

This equation reflects the mean value of bed shear stress due to waves and currents over the wave cycles (Whitehouse et al., 2000).

It is necessary to indicate that, in the presence of waves, the wave and current effects are difficult to clearly separate, due to their nonlinear interaction. Therefore, the above method may need to be improved in future studies. However, in the present study, we focus on the typhoon impact by comparing the τ_{cw} values during storm and calm weathers. The systematic errors, if there are, unlikely would affect the reliability of our comparison.

The critical shear stress for erosion (τ_e, N/m^2) is given by (Taki, 2001):

$$\tau_e = 0.05 + \beta\left[\frac{1}{\{(\pi/6)(1+sW)\}^{1/3} - 1}\right]^2 \tag{A8}$$

where β ($=0.3$) is an electrochemical anchoring coefficient, s ($=\rho_s/\rho_w$, where ρ_s and ρ_w are the density of bed sediment ($=2650\ kg/m^3$) and seawater ($=1028\ kg/m^3$), respectively) is the specific weight of sediment (Shi et al., 2017), and W is the water content of sediment sample defined as the ratio of water weight to dry sediment weight, expressed as a percentage (measured in the laboratory).

Appendix B. Supplementary data

Supplementary data to this article can be found online at https://doi.org/10.1016/j.jhydrol.2019.05.077.

References

Alvarez, L.G., 2010. Bottom boundary layer properties in the Upper Gulf of California derived from velocity profiles. Ciencias Mar. 36, 285–299. https://doi.org/10.7773/cm.v36i3.1760.

Barbier, E.B., Hacker, S.D., Kennedy, C., Koch, E.W., Stier, A.C., Silliman, B.R., 2011. The value of estuarine and coastal ecosystem services. Ecol. Monogr. 81, 169–193. https://doi.org/10.1890/10-1510.1.

Blankespoor, B., Dasgupta, S., Laplante, B., 2014. Sea-level rise and coastal wetlands. AMBIO 43, 996–1005. https://doi.org/10.1007/s13280-014-0500-4.

Blum, M.D., Roberts, H.H., 2009. Drowning of the Mississippi Delta due to insufficient sediment supply and global sea-level rise. Nat. Geosci. 2, 488–491. https://doi.org/10.1038/ngeo553.

Bridges, K.H.P., 1987. Coriolis effect. In: Climatology. Springer US, Boston, MA, pp. 370. https://doi.org/10.1007/0-387-30749-4_57.

Call, M., Maher, D.T., Santos, I.R., Ruiz-Halpern, S., Mangion, P., Sanders, C.J., et al., 2015. Spatial and temporal variability of carbon dioxide and methane fluxes over semi-diurnal and spring–neap–spring timescales in a mangrove creek. Geochim. Cosmochim. Acta 150, 211–225. https://doi.org/10.1016/j.gca.2014.11.023.

Chang, Y.C., Chen, G.Y., Tseng, R.S., Centurioni, L.R., Chu, P.C., 2012. Observed near-surface currents under high wind speeds. J. Geophys. Res. Ocean. 117, 1–6. https://doi.org/10.1029/2012JC007996.

Costanza, R., d'Arge, R., de Groot, R., Farber, S., Grasso, M., Hannon, B., et al., 1997. The value of the world's ecosystem service and natural capital. Nature 387, 253–260. https://www.nature.com/articles/387253a0.pdf.

Donnelly, J.P., Butler, J., Roll, S., Wengren, M., Iii, T.W., 2004. A backbarrier overwash record of intense storms from Brigantine, New Jersey. Mar. Geol. 210, 107–121. https://doi.org/10.1016/j.margeo.2004.05.005.

Emanuel, K., 2005. Increasing destructiveness of tropical cyclones over the past 30 years 436, 686–688. doi: 10.1038/nature03906.

Fredsøe, J., 1984. Turbulent boundary layer in wave-current motion. J. Hydraul. Eng. 110, 1103–1120. https://doi.org/10.1061/(ASCE)0733-9429(1984) 110.

Gao, A., Zhao, H.Y., Yang, S.L., Dai, S.B., Chen, S.L., Li, P., 2008. Seasonal and tidal variations in suspended sediment concentration under the influence of river runoff, tidal current and wind waves: taking the Nanhui Headland, the joint area between Changjiang Estuary and Hangzhou Bay as an example. Adv. Mar. Sci. 26 (1), 44–50. http://www.airitilibrary.com/Publication/alDetailedMesh?docid=16716647-

200801-26-1-44-50-a.
Kirwan, M.L., Megonigal, J.P., 2013. Tidal wetland stability in the face of human impacts and sea-level rise. Nature 504, 53–60. https://doi.org/10.1038/nature12856.
Knutson, T.R., McBride, J.L., Chan, J., Emanuel, K., Holland, G., Landsea, C., et al., 2010. Tropical cyclones and climate change. Nat. Geosci. 3, 157. https://doi.org/10.1002/wcc.371.
Komar, P.D., 1976. Beach Processes and Sedimentation. Prentice-Hall, Englewood Cliffs, New Jersey.
Leonardi, N., Ganju, N.K., Fagherazzi, S., 2016. A linear relationship between wave power and erosion determines salt-marsh resilience to violent storms and hurricanes. Proc. Natl. Acad. Sci. 113, 64–68. https://doi.org/10.1073/pnas.1510095112.
Leonardi, N., Carnacina, I., Donatelli, C., Ganju, N.K., Plater, A.J., Schuerch, M., et al., 2018. Dynamic interactions between coastal storms and salt marshes: a review. Geomorphology 301, 92–107. https://doi.org/10.1016/j.geomorph.2017.11.001.
Liu, K., Bianchette, T., Zou, L., Qiang, Y., Lam, N., 2017. Contribution of recent hurricanes to wetland sedimentation in coastal Louisiana. Austria In: EGU General Assembly Conference (Vol.19). Geophysical Research Abstracts, pp. 12001. http://adsabs.harvard.edu/abs/2017EGUGA..1912001L.
Osborne, P.D., Greenwood, B., 2010. Sediment suspension under waves and currents: time scales and vertical structure. Sedimentology 40, 599–622. https://doi.org/10.1111/j.1365-3091.1993.tb01352.x.
Schuerch, M., Spencer, T., Temmerman, S., Kirwan, M.L., Wolff, C., Lincke, D., et al., 2018. Future response of global coastal wetlands to sea-level rise. Nature 561, 231. https://doi.org/10.1038/s41586-018-0476-5.
Shaikh, N., Siddiqui, K., 2011. Near-surface flow structure over wind-generated water waves, part I: wave-induced flow characteristics. Ocean Dyn. 61, 127–141. https://doi.org/10.1007/s10236-010-0361-8.
Shi, B., Cooper, J.R., Pratolongo, P.D., Gao, S., Bouma, T.J., Li, G., et al., 2017. Erosion and accretion on a mudflat: the importance of very shallow-water effects. J. Geophys. Res. Ocean. 122. https://doi.org/10.1002/2016JC012316.
Sobel, A.H., Camargo, S.J., Hall, T.M., Lee, C., Tippett, M.K., Wing, A.A., 2016. Human influence on tropical cyclone intensity. Science 353 (6296), 242–246. https://doi.org/10.1126/science.aaf6574.
Soulsby, R.L., 1995. Bed shear-stress due to combined waves and currents. In: Stive, M.J.F. (Ed.), Advances in Coastal Morphodynamics, 4-20 to 4-23, Delft Hydraul., Delft, Netherlands (after Whitehouse et al., 2002).
Soulsby, R.L., 1997. Dynamics of marine sands: a manual for practical applications. Dyn. Mar. Sands a Man. Pract. Appl. 249. doi: 10.1680/doms.25844.
Sun, Y., Dong, C., He, Y., Yu, K., Renault, L., Ji, J., 2016. Seasonal and Interannual Variability in the Wind-Driven Upwelling Along the Southern East China Sea Coast 9, 1–8. doi: 10.1109/JSTARS.2016.2544438.
Taki, K., 2001. Critical shear stress for cohesive sediment transport. Proc. Mar. Sci. 3, 53–61. https://doi.org/10.1016/S1568-2692(00)80112-6.
Temmerman, S., Meire, P., Bouma, T.J., Herman, P.M.J., Ysebaert, T., De Vriend, H.J., 2013. Ecosystem-based coastal defence in the face of global change. Nature 504, 79–83. https://doi.org/10.1038/nature12859.
Turner, R.E., Baustian, J.J., Swenson, E.M., Spicer, J.S., 2006. Wetland sedimentation from hurricanes Katrina and Rita. Science 314, 449–452. https://doi.org/10.1126/science.1129116.
Van Ormondt, M., Hapke, C., Roelvink, D., Nelson, T.R., 2015. The effects of geomorphic changes during Hurricane Sandy on water levels in Great South Bay. In: The Proceedings of the Coastal Sediments 2015. World Sci., Singapore, pp. 14. https://doi.org/10.1142/9789814689977_0221.
Van Rijn, L.C., 1993. Principles of Sediment Transport in Rivers, Estuaries and Coastal Seas. Aqua Publication, Amsterdam, The Netherlands.
Wang, T., Liu, G., Gao, L., Zhu, L., Fu, Q., Li, D., 2016. Biological and nutrient responses to a typhoon in the yangtze estuary and the adjacent sea. J. Coast. Res. 32, 323–332. https://doi.org/10.2112/jcoastres-d-15-00006.1.
Wang, F., Yu, Z., Xu, B., Liu, J., Guo, X., Nan, H., 2018. Nepartak typhoon influenced bottom sediments from the yangtze river estuary and adjacent east china sea-foraminiferal evidence. Geochem. Geophys. Geosyst. 1049–1063. https://doi.org/10.1002/2017GC007413.
Weber, J.E., 1983. Steady wind-and wave-induced currents in the open ocean. J. Phys. Oceanogr. https://doi.org/10.1175/1520-0485(1983) 013<0524:SWAWIC>2.0.CO;2.
Webster, P.J., Holland, G.J., Curry, J.A., Chang, H.-R., 2005. Changes in tropical cyclone number, duration, and intensity in a warming environment. Science 309, 1844–1846. https://doi.org/10.1126/science.1116448.
Whitehouse, R., Soulsby, R.L., Roberts, W., 2000. Dynamics of Estuarine Muds: A Manual for Practical Applications. Thomas Telford, London ISBB 0727728644, 9780727728647.
Williams, H.F.L., Flanagan, W.M., 2009. Contribution of hurricane rita storm surge deposition to long-term sedimentation in louisiana coastal woodlands and marshes. J. Coast. Res. 2009, 1671–1675. https://doi.org/10.1111/j.1467-8330.2010.00820.x.
Wu, J., 1975. Wind-induced drift currents. J. Fluid Mech. 68, 49–70. https://doi.org/10.1017/S0022112075000687.
Yang, S.L., Eisma, D., Ding, P.X., 2000. Sedimentary processes on an estuarine marsh island within the turbidity maximum zone of the Yangtze river mouth. Geo-Marine Lett. 20, 87–92. https://doi.org/10.1007/s003670000042.
Yang, S.L., Friedrichs, C.T., Shi, Z., Ding, P.X., Zhu, J., Zhao, Q.Y., 2003. Morphological response of tidal marshes, flats and channels of the outer yangtze river mouth to a major storm. Estuaries 26, 1416–1425. https://doi.org/10.1007/BF02803650.
Yang, S.L., Li, H., Ysebaert, T., Bouma, T.J., Zhang, W.X., Wang, Y.Y., et al., 2008. Spatial and temporal variations in sediment grain size in tidal wetlands, Yangtze Delta: On the role of physical and biotic controls. Estuar. Coast. Shelf Sci. 77, 657–671. https://doi.org/10.1016/j.ecss.2007.10.024.
Yang, S.L., Shi, B.W., Bouma, T.J., Ysebaert, T., Luo, X.X., 2012. Wave attenuation at a salt marsh margin: a case study of an exposed coast on the yangtze estuary. Estuar. Coasts 35, 169–182. https://doi.org/10.1007/s12237-011-9424-4.
Yang, H.F., Yang, S.L., Xu, K.H., Milliman, J.D., Wang, H., Yang, Z., et al., 2018. Human impacts on sediment in the Yangtze River: a review and new perspectives. Global Planet. Change 162, 8–17. https://doi.org/10.1016/j.gloplacha.2018.01.001.
Yang, S.L., Zhang, J., Zhu, J., Smith, J.P., Dai, S.B., Gao, A., 2005. Impact of dams on yangtze river sediment supply to the sea and delta wetland response. J. Geophys. Res. 110, F03006. https://doi.org/10.1029/2004JF000271.
Zhu, Q., Yang, S.L., Ma, Y.X., 2014. Intra-tidal sedimentary processes associated with combined wave–current action on an exposed, erosional mudflat, southeastern Yangtze River Delta China. Mar. Geol. 347, 95–106. https://doi.org/10.1016/j.margeo.2013.11.005.
Zhu, Q., Prooijen, B.C. Van, Wang, Z.B., Ma, Y.X., Yang, S.L., 2016. Bed shear stress estimation on an open intertidal flat using in situ measurements. Estuar. Coast. Shelf Sci. 182, 190–201. https://doi.org/10.1016/j.ecss.2016.08.028.
Zhu, Q., Prooijen, B.C. Van, Wang, Z.B., Yang, S.L., 2017. Bed-level changes on intertidal wetland in response to waves and tides: a case study from the Yangtze River Delta. Mar. Geol. 385, 160–172. https://doi.org/10.1016/j.margeo.2017.01.003.